ISSN 1054-660X, Laser Physics, 2012, Vol. 22, No. 10, pp. 1565–1572.

Dual-Wavelength Operation of a Figure-Eight Fiber Laser[1]

O. Pottiez[a], *, J. C. Hernandez-Garcia[a], B. Ibarra-Escamilla[b], and E. A. Kuzin[b]

[a] *Centro de Investigaciones en Óptica (CIO), Loma del Bosque 115, Col. Lomas del Campestre, León, Gto. 37150, Mexico*

[b] *Instituto Nacional de Astrofísica, Óptica y Electrónica (INAOE), Departamento de Óptica, L.E. Erro 1, Puebla, Pue. 72000, Mexico*

*e-mail: pottiez@cio.mx

Received October 5, 2011; in final form, October 11, 2011; published online September 3, 2012

Abstract—We study numerically an erbium-doped figure-eight fiber laser including a double-bandpass optical filter for dual-wavelength pulse generation. Simulations are performed for several values of the filter bandwidth and wavelength separation between the transmission windows. The results show that dual-wavelength mode-locking is obtained in most cases, with a balanced energy distribution between wavelengths. Due to cavity dispersion, the pulses at each wavelength are asynchronous for a large wavelength separation, whereas they are synchronous for closely spaced wavelengths, as in this case cross-phase modulation is able to compensate for the dispersion-induced walkoff. In the asynchronous case, dual-wavelength operation is favored by the filter loss, whereas in the synchronous case it is favored by the saturable absorber action of the nonlinear optical loop mirror. Simulations also show that, thanks to those stabilization mechanisms, dual-wavelength pulsed operation does not require precise cavity loss equalization between the two oscillating wavelengths.

DOI: 10.1134/S1054660X12100180

1. INTRODUCTION

Whereas Q-switched lasers are able to produce long high-energy pulses [1, 2], the mode locking technique is better suited for the generation of ultrashort optical pulses, whose durations typically range from tens of femtoseconds to a few picoseconds, although longer durations are not excluded [3–5]. Because of their ability to generate pulse trains at several wavelengths simultaneously, multiple-wavelength mode-locked fiber lasers are attractive sources for several applications including Wavelength Division Multiplexing (WDM) transmissions, signal processing, or sensing. In particular, multiple-wavelength operation of actively mode-locked fiber lasers was demonstrated, including in the cavity comb-like filtering elements like a Fabry–Perot filter [6], cascaded or superimposed fiber Bragg gratings [7–12], a birefringent Sagnac interferometer or a piece of birefringent fiber in combination with polarizers [13, 14]. Besides the choice of the optical filter, a fundamental parameter that affects the spectral behavior of the laser is the nature of the amplifying medium [15]. Hence, in erbium-doped fiber lasers, contrary to semiconductor optical amplifier (SOA) based lasers [16], an issue is the homogeneous broadening of the gain medium, which triggers gain competition and makes it difficult to maintain lasing at different wavelengths simultaneously. Solutions to counteract gain competition have been found however, although some of them are difficult to implement or expensive, like the use of multiple amplifiers in the laser [7, 12] or cooling the system down to cryogenic temperatures in order to reduce the gain homogeneous bandwidth [17]. Fortunately, some much more practical solutions have been proposed, like the use of spatial hole burning [18] or polarization hole burning [19] in the doped fiber, frequency shifting [6], reduction of temporal overlap between different wavelengths in the amplifier [11, 20] or the use of nonlinearities in fibers to introduce an intensity-limiting effect, like four wave mixing [21], nonlinear polarization rotation [22] or Stimulated Brillouin scattering [23]. An additional issue is the synchronization of pulse trains at different wavelengths with the reference signal, which is not trivial in presence of fiber dispersion [10, 21, 24].

A clear advantage of actively mode-locked fiber lasers is their ability to generate pulse trains at well defined (and usually high) repetition rates, thanks to the use of an external oscillator. Therefore they are more attractive than passively mode-locked lasers for some applications like optical transmissions. For other applications however, the use of passively mode-locked sources, which do not require such an external reference, usually means a substantial economy. As a consequence, research on passively mode-locked fiber lasers remains very active today, benefiting in particular from the introduction of novel technologies, like for example carbon nanotubes [25, 26] and bismuth-based fibers [26, 27]. For this reason, it may appear surprising that relatively few references can be found on dual-wavelength passively mode-locked fiber lasers [28–35]. In [29], dual-wavelength pulsed operation

[1] The article is published in the original.

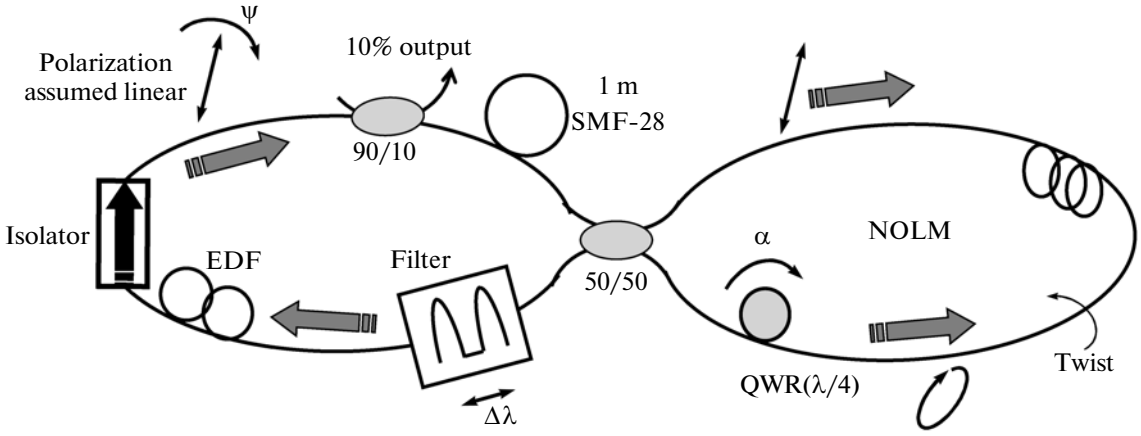

Fig. 1. Scheme of the laser under study. EDF: erbium-doped fiber.

was obtained at the price of a precise equalization of the losses for the two wavelengths. It seems that the lack of interest for developing multiple wavelength passively mode-locked sources may find a partial explanation in the common belief that gain competition makes it difficult and pricy to get a stable operation of these lasers in which two or more wavelengths oscillate simultaneously.

In this paper, we study numerically a passively mode-locked figure-eight fiber laser including a double-bandpass filter, and present results that tend to demonstrate that dual-wavelength operation of this laser may be at least as easy to obtain as single-wavelength operation, thanks to the operation of the filter and of the nonlinear optical loop mirror (NOLM).

2. MODEL

The laser under study is shown in Fig. 1. It is a figure-eight scheme, including a ring section (left) and a Nonlinear Optical Loop Mirror (NOLM, on the right), which is responsible for mode locking [36]. Its total length is 7 m. The dispersion and nonlinear Kerr coefficient of all pieces of fiber considered in the numerical study are $D = 17$ ps nm^{-1} km^{-1} and $\gamma = 1.5$ W^{-1} km^{-1} (for linear polarization), respectively. The ring section includes a 3-m long Erbium-doped fiber (EDF) amplifier, whose gain is assumed to be homogeneously broadened. The ring section also includes an isolator, a 90/10 output coupler and a double Gaussian bandpass filter with wavelength separation $\Delta\lambda$ (e.g., two superposed fiber Bragg gratings inserted through a circulator). The pigtails of these components were accounted for by including a 1-m piece of standard fiber at the NOLM input. Contrary to conventional, power-asymmetric schemes [37], the NOLM operates through nonlinear polarization rotation (NPR) instead of self-phase modulation. It includes a 50/50 coupler, a 3-m piece of twisted standard fiber (twist = 3 turns/m, which is used to reduce the effects of residual fiber birefringence) and a quarter-wave retarder (QWR) inserted asymmetrically in the loop. Although the device is power-symmetric, it is polarization-imbalanced through the QWR. As NPR depends on light polarization, it provides a mechanism for switching even when the counter-propagating beams have equal powers. This NOLM was first proposed in [38], and its capabilities have been analyzed both theoretically [39] and experimentally [40], showing in particular the flexibility of its transmission characteristic, which can be adjusted through QWR orientation and input polarization selection. In particular, the QWR angle α allows adjusting the low-power NOLM transmission. In this work, polarization at the NOLM input is assumed to be linear (this can be easily implemented in practice using a polarization controller and a polarizer at the NOLM input). In this case, the NOLM switching power can be adjusted through the angle ψ of input polarization [39, 40]. In this numerical study, the angle α was adjusted to have a small though nonzero low-power NOLM transmission of ~0.05 (for proper mode locking, low-power transmission should be small yet different from zero, so that the laser oscillation can initiate from low-power noise). The NOLM input polarization angle ψ is set to 45° with respect to the QWR axes, yielding a circularly polarized counter-clockwise beam and, with the fiber parameters mentioned above, a minimal switching power of ~4000 W.

The operation of the laser is studied through numerical simulations. Propagation is modeled thanks to a set of two coupled nonlinear Schrödinger equations, which are integrated using the Split–Step

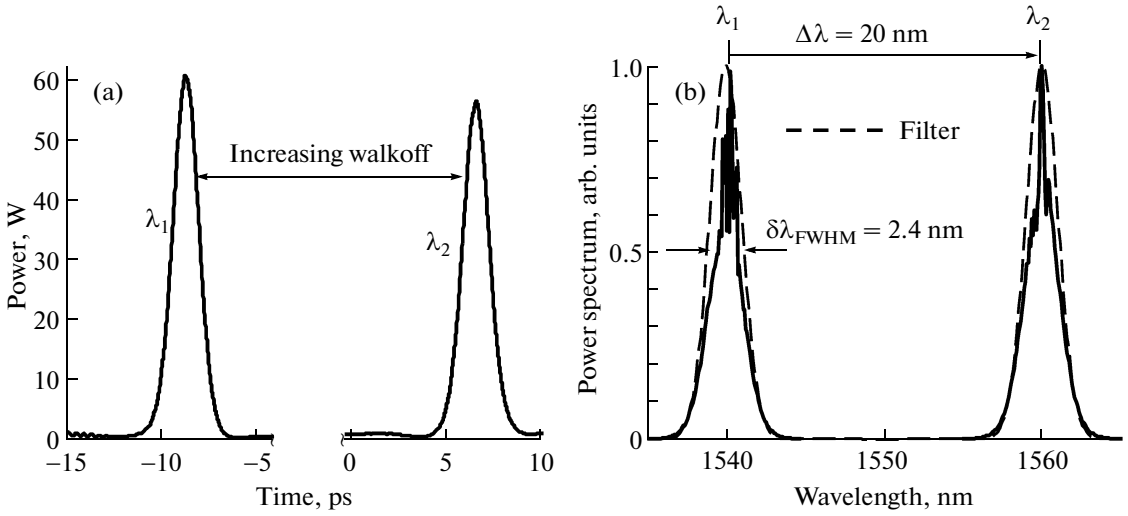

Fig. 2. (a) Temporal profile and (b) optical spectrum of the laser output signal for $\Delta\lambda = 20$ nm, $\delta\lambda_{FWHM} = 2.4$ nm, and $\varepsilon = 0$.

Fourier (SSF) method. In the circular polarization basis $[C^+, C^-]$, these equations write as [41]

$$\frac{\partial C^+}{\partial z} = -j\frac{\beta_2}{2}\frac{\partial^2 C^+}{\partial t^2} + \frac{2}{3}j\gamma(|C^+|^2 + 2|C^-|^2)C^+ + \frac{g}{2}C^+;$$
$$\frac{\partial C^-}{\partial z} = -j\frac{\beta_2}{2}\frac{\partial^2 C^-}{\partial t^2} + \frac{2}{3}j\gamma(|C^-|^2 + 2|C^+|^2)C^- + \frac{g}{2}C^-, \quad (1)$$

where C^+ and C^- are the circular right and left polarization components, respectively. The first two right-hand terms of Eq. (1) are dispersive and Kerr nonlinear terms (the latter including self-and cross-phase modulation). The third terms are gain terms, which are considered only for integration over the gain section. The coefficient g is the gain per unit length. Here g is assumed to be constant across the doped fiber, and saturates on the pulse energy E_p as

$$g(E_p) = \frac{g_0}{1 + E_p/E_{sat}}, \quad (2)$$

where g_0 is the small-signal gain and E_{sat} is the saturation energy. For the simulations presented here, we use $g_0 = 1333/m$ and E_{sat} values range between 0.03 and 0.20 nJ. The spectral dependence of gain is not considered, as its bandwidth is assumed to be larger than the bandwidth of the filters. For the double-bandwidth filter, the following power spectral transmission was used:

$$F(\lambda) = \exp\left[-\left(\frac{\lambda - \lambda_1}{\delta\lambda_{FWHM}/1.66}\right)^2\right] + (1-\varepsilon)\exp\left[-\left(\frac{\lambda - \lambda_2}{(\delta\lambda_{FWHM}/1.66)}\right)^2\right]. \quad (3)$$

The values of the full-width at half maximum (FWHM) filter bandwidth $\delta\lambda_{FWHM}$ and wavelength separation $\Delta\lambda = \lambda_2 - \lambda_1$ were the parameters of simulation. The parameter $\varepsilon < 1$ was introduced to simulate a difference of cavity losses between λ_1 and λ_2 ($\varepsilon = 0$ for balanced losses). Finally, the twist-induced group-velocity mismatch between circular polarization components, as well as higher-order effects like the Raman self-frequency shift and third-order dispersion were not accounted for, as it was observed that they have no noticeable effect on the results for the parameters used in the simulations.

For each set of laser parameters, a small-amplitude Gaussian noise is chosen as the initial signal. This signal is propagated over several cycles, and we observe whether a steady-state can be reached or not after a finite number of integration cycles.

3. RESULTS AND DISCUSSION

Although a strict-sense convergence is not obtained for some sets of simulation parameters, a relatively stable pulsing behavior was generally obtained in regime, although substantial amplitude fluctuations remain in some cases. The nature of the pulses strongly depends on the filter properties, however in a large majority of situations a dual-wavelength pulsed operation of the laser is readily observed.

Figure 2 presents simulation results for $\Delta\lambda = 20$ nm, $\delta\lambda_{FWHM} = 2.4$ nm and $\varepsilon = 0$. Two temporally separated pulses are obtained in regime, one with a spectrum centered at λ_1 and the other one at λ_2. The pulses have nearly the same amplitude with a FWHM duration = 1.6 ps and a FWHM bandwidth of 2 nm. This corresponds to a time-bandwidth product of 0.42, showing that the pulses are slightly chirped (assuming a squared sech profile). Due to anomalous

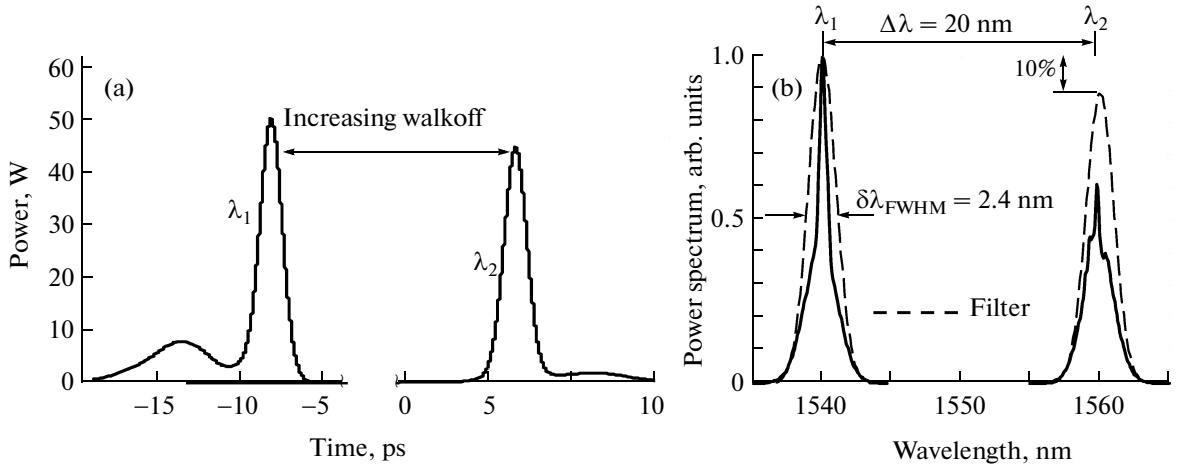

Fig. 3. (a) Temporal profile and (b) optical spectrum of the laser output signal for $\Delta\lambda = 20$ nm, $\delta\lambda_{FWHM} = 2.4$ nm, and $\varepsilon = 0.1$.

cavity dispersion and the large wavelength difference, these pulses are unsynchronized, i.e., their temporal separation increases monotonically with successive round-trips (walkoff). Apart from this walkoff, the pulses are found to be stable in regime, maintaining indefinitely roughly equal amplitudes.

The stability of unsynchronized dual-wavelength pulsed operation against single-wavelength pulsing in the previous example can be explained as follows. The mode of operation of the laser that eventually prevails is determined by the balance between two effects. First, the NOLM saturable absorber action introduces higher cavity losses for low-intensity components of the optical signal. Therefore, the NOLM favors a mode of operation in which all available energy is concentrated in one single pulse, for which the peak power is higher and which suffers lower losses than in the case of two nearly equal pulses. This is valid as far as the pulse peak power at the NOLM input remains well below the NOLM switching power (which guarantees that the NOLM acts as saturable absorber and not as intensity limiter). Considering the very large NOLM switching power in comparison with the pulse peak power values obtained in these results (at the NOLM input, where peak power is ~9 times the value at the laser output, see Fig. 1), this criterion is clearly met. The second key effect is the intracavity loss generated by the double-bandpass filter. In the anomalous-dispersive nonlinear (solitonic) regime, a high-energy single pulse is temporally shorter, and thus spectrally broader than two lower-energy pulses. Therefore, the former will suffer higher losses through the bandpass filter. As a result, the double-bandpass filter favors the coexistence of two pulses, one at λ_1 and the other one at λ_2, with nearly equal amplitudes so as to minimize the losses through the filter. In the case of Fig. 2, where the filter bandwidth is relatively narrow, the signal spectrum tends to fill all the available bandwidth (see Fig. 2b, where the dashed curve materializes the filter spectrum), and any spectral widening of the signal dramatically increases the losses through the filter. In this case, the filtering effect tends to dominate over the NOLM effect, and the laser operates in the dual-wavelength asynchronous pulsed regime.

In practice, intracavity losses can vary substantially with wavelength, causing the pulses at λ_1 and λ_2 to suffer unequal losses through the cavity, which in turn could affect the dual-wavelength operation. In order to assess the stability of dual-wavelength lasing against such a loss difference, we repeated the simulation of Fig. 2 with the same filter parameters, except that we now chose $\varepsilon = 0.1$. Figure 3 shows that this substantial loss difference does not affect severely the dual-wavelength pulsing. In particular, the pulses conserve nearly equal amplitudes in this case. This result is remarkable and demonstrates the outstanding stabilizing capabilities of the dual filter in the mode-locked regime. In comparison, in the continuous-wave regime of fiber lasers, due to homogeneous broadening of the gain medium, dual-wavelength operation often requires careful intracavity loss adjustments [42–44]. For example, it was shown experimentally that, for stable dual-wavelength operation of a continuous-wave erbium-doped fiber laser, the tolerance on the loss difference between both wavelengths is as small as ~1% [45].

In order to confirm the key role of filter losses in stabilizing asynchronous dual-wavelength operation, we increased significantly the filter bandwidth ($\delta\lambda_{FWHM} = 6$ nm). In this case, again with $\Delta\lambda = 20$ nm, and even assuming balanced cavity losses ($\varepsilon = 0$), a single pulse at only one wavelength (either λ_1 or λ_2) was found in regime (Fig. 4). Indeed, in this case the wide available optical bandwidth can hardly impose any substantial loss on the pulse, whose spectrum is now narrower than the filter (see Fig. 4b). Under such

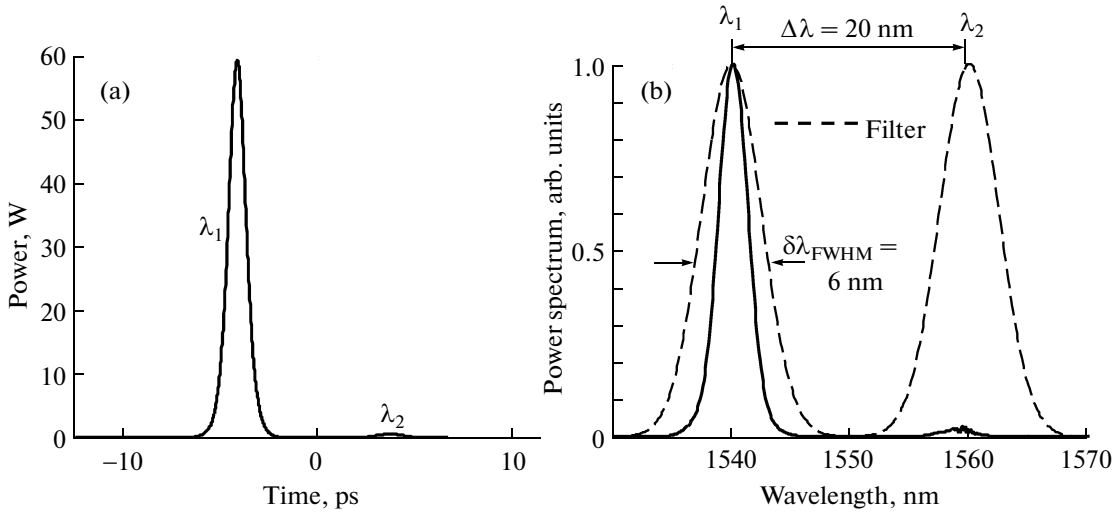

Fig. 4. (a) Temporal profile and (b) optical spectrum of the laser output signal for $\Delta\lambda = 20$ nm, $\delta\lambda_{FWHM} = 6$ nm, and $\varepsilon = 0$.

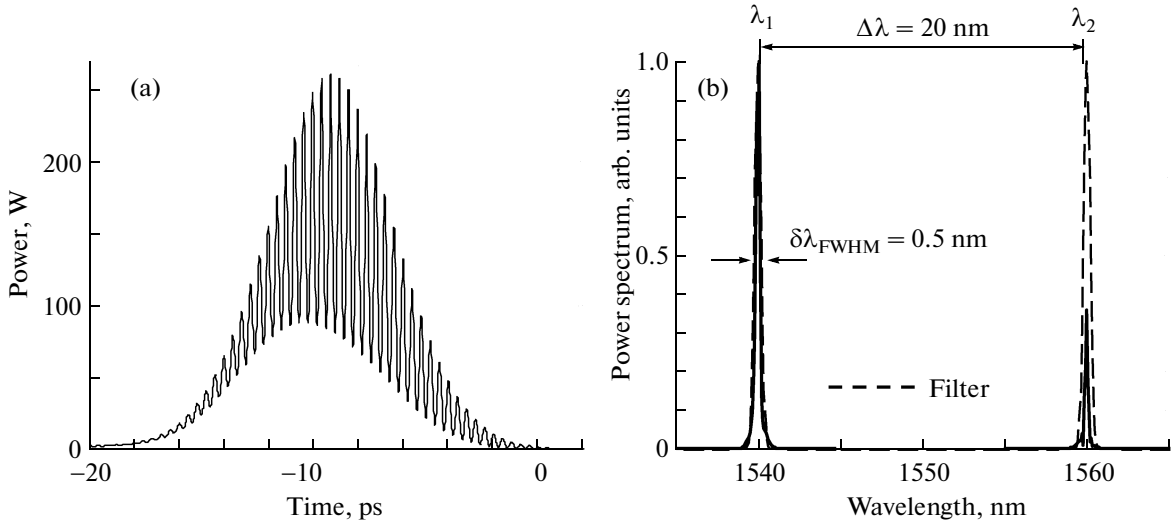

Fig. 5. (a) Temporal profile and (b) optical spectrum of the laser output signal for $\Delta\lambda = 20$ nm, $\delta\lambda_{FWHM} = 0.5$ nm and $\varepsilon = 0$.

circumstances, the NOLM prevails in determining the laser operation and a single-wavelength single pulse is obtained.

Symmetrically, we analyzed the effect of narrowing the filter bandwidth (see Fig. 5, for $\delta\lambda_{FWHM} = 0.5$ nm, $\Delta\lambda = 20$ nm, and $\varepsilon = 0$). In this case, two-wavelength operation reappears, although the energy distribution between the two wavelengths tends to be largely imbalanced and unstable. In the temporal domain, it is noticeable that two asynchronous pulses are no longer formed, but instead a single large (~6-ps) pulse, modulated in amplitude by the beat tone corresponding to the frequency difference between its two spectral components. The large pulse duration is related to the very narrow filter bandwidth. Synchronism is obtained as a consequence of nonlinear cross-phase modulation (XPM) between the two wavelengths, which opposes the dispersion-induced walkoff [41]. Although the wavelength separation is still as large as previously, a larger pulse duration and higher peak power allow XPM to counteract the walkoff, avoiding that the two wavelength components be pulled apart.

Synchronous double-wavelength pulsed operation can be better illustrated and understood with the following example. Here we assume $\Delta\lambda = 4$ nm, $\delta\lambda_{FWHM} = 1$ nm and $\varepsilon = 0$ (Fig. 6). Due to reduced wavelength separation, the dispersion-induced walkoff is smaller and is easily compensated by XPM in this ~5 ps pulse. Again, the beat tone at the frequency difference between the two spectral compo-

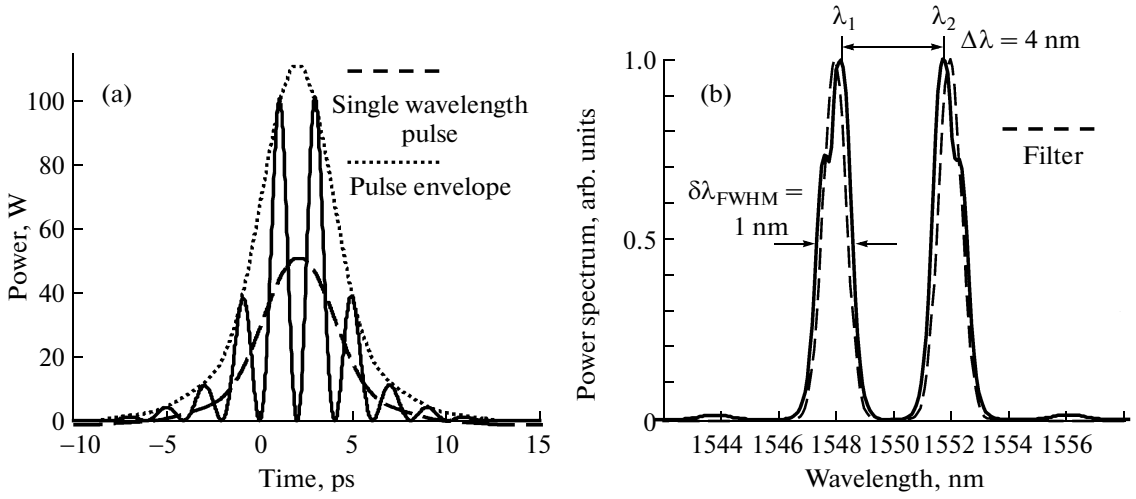

Fig. 6. (a) Temporal profile and (b) optical spectrum of the laser output signal for $\Delta\lambda = 4$ nm, $\delta\lambda_{FWHM} = 1$ nm, and $\varepsilon = 0$.

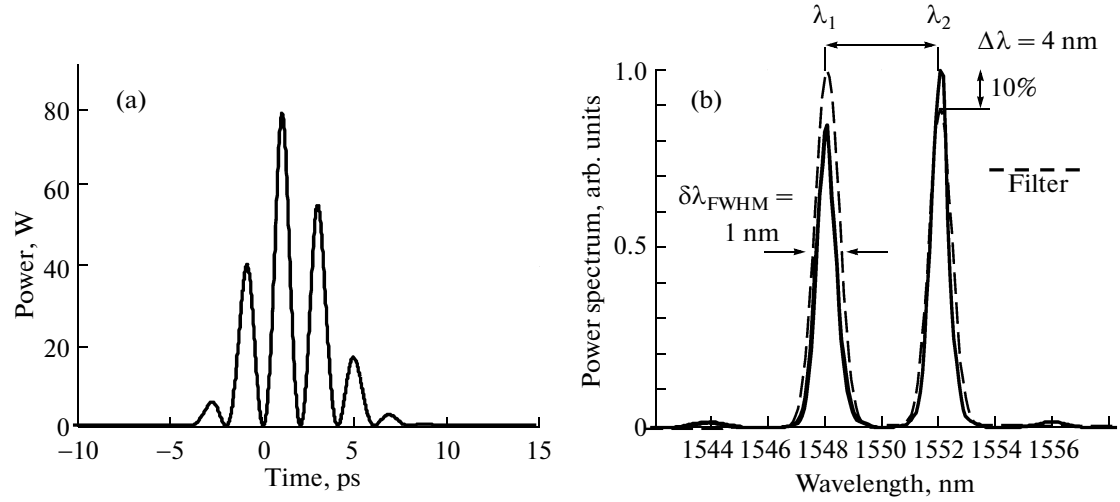

Fig. 7. (a) Temporal profile and (b) optical spectrum of the laser output signal for $\Delta\lambda = 4$ nm, $\delta\lambda_{FWHM} = 1$ nm, and $\varepsilon = 0.1$.

nents modulates the pulse profile. In this case however, it is noteworthy that both spectral contributions are nearly equal (yielding a 100% modulation depth in the time domain). In the synchronous case, it is not clear whether the filter favors single- or dual-wavelength operation. In contrast, the role of the NOLM is clear, and opposite to the synchronous case. Indeed, let us consider a single-wavelength pulse having the same energy (determined by gain saturation energy) and duration (limited by filter bandwidth) as the actual dual-wavelength pulse. This pulse is shown in Fig. 6a, dashed line. It appears that the peak power of this single-wavelength pulse is about half that of the dual-wavelength synchronous waveform. As a consequence, transmission through the NOLM is smaller for this pulse than for the dual-wavelength one. Therefore, in the synchronous case, the NOLM saturable absorber action favors dual-wavelength operation, contrary to the asynchronous case. Besides, the peak power of the dual-wavelength pulse (and thus the NOLM transmission) is maximal when the modulation depth of the beat tone is 100%, i.e., when spectral contributions at both wavelengths are equal, which ensures a balanced energy repartition between the two wavelengths. Again, the robustness of this mode of operation against cavity loss differences was demonstrated by repeating the simulation with $\varepsilon = 0.1$ (results shown in Fig. 7). Note that, once more, the values of pulse peak power at the NOLM input in all cases remains well below the NOLM switching power, so that the NOLM action is never intensity-limiting.

4. CONCLUSIONS

In conclusion, we performed a numerical study of an Erbium-doped figure-eight fiber laser including a double-bandpass filter for the generation of ultrashort pulses at two wavelengths simultaneously. Simulations were carried out for various values of wavelength separation and bandwidth of the filter transmission windows. In most cases, dual-wavelength pulsed operation is observed, either synchronous or asynchronous, with a rather symmetric repartition of energy between the two wavelengths. The mechanism allowing dual-wavelength pulsing to prevail over single-wavelength operation is found to be the filter losses in the asynchronous case, and the NOLM saturable absorber action in the synchronous case. Single-wavelength operation was only observed in the asynchronous case, when the filter bandwidth is large compared to the signal bandwidth, causing no substantial losses on the pulse. Asynchronous dual pulsing is caused by fiber dispersion, which is responsible for a group velocity difference between pulses at different wavelengths, creating a walkoff that increases monotonically with successive round-trips. For moderate values of the wavelength difference however, this dispersion-induced walkoff can be compensated by XPM, the faster pulse tending to accelerate the slower one and conversely. In this case, synchronous dual-wavelength operation is observed, and the pulse envelope is amplitude-modulated at the beat frequency. Finally, these results also show that dual-wavelength operation is robust against a spectral dependence of cavity losses, and therefore does not require a precise cavity loss adjustment between the two wavelengths. Indeed, a difference as high as 10% does not significantly alter dual-wavelength operation nor the energy balance between the two wavelengths. These results can be useful to cast a new light on the problem of designing multiple-wavelength passively mode-locked lasers, which are useful for a wide range of applications.

ACKNOWLEDGMENTS

O. Pottiez was supported by CONACyT grant 130681.

REFERENCES

1. J. F. Yang, S. D. Liu, J. L. He, et al., Laser Phys. Lett. **8**, 28 (2011).
2. A. S. Kurkov, Ya. E. Sadovnikova, A. V. Marakulin, and E. M. Sholokhov, Laser Phys. Lett. **7**, 795 (2010).
3. I. L. Villegas, C. Cuadrado-Laborde, J. Abreu-Afonso, et al., Laser Phys. Lett. **8**, 227 (2011).
4. B. N. Nyushkov, V. I. Denisov, S. M. Kobtsev, et al., Laser Phys. Lett. **7**, 661 (2010).
5. L. J. Kong, X. S. Xiao, and C. X. Yang, Laser Phys. Lett. **7**, 359 (2010).
6. J.-N. Maran, S. Larochelle, and P. Besnard, Opt. Lett. **28**, 2082 (2003).
7. D. A. Pattison, P. N. Kean, J. W. D. Gray, et al., IEEE Photon. Technol. Lett. **7**, 1415 (1995).
8. Y. Zhao and C. Shu, Appl. Phys. Lett. **72**, 1556 (1998).
9. S. Li, H. Ding, and K. T. Chan, Electron. Lett. **33**, 390 (1997).
10. O. Deparis, R. Kiyan, E. Salik, er al., IEEE Photon. Technol. Lett. **11**, 1238 (1999).
11. G. E. Town, L. Chen, and P. W. E. Smith, IEEE Photon. Technol. Lett. **12**, 1459 (2000).
12. D. Pudo and L. R. Chen, Electron. Lett. **39**, 272 (2003).
13. J. B. Schlager, S. Kawanishi, and M. Saruwatari, Electron. Lett. **27**, 2072 (1991).
14. H. Takara, S. Kawanishi, M. Saruwatari, and J. B. Schlager, Electron. Lett. **28**, 2274 (1992).
15. A. V. Kir'yanov and N. N. Il'ichev, Laser Phys. Lett. **8**, 305 (2011).
16. A. A. Latif, M. Z. Zulkifli, N. A. Hassan, et al., Laser Phys. Lett. **7**, 597 (2010).
17. R. Hayashi, S. Yamashita, and T. Saida, IEEE Photon. Technol. Lett. **15**, 1692 (2003).
18. Y. Yao, X. Chen, Y. Dai, and S. Xie, IEEE Photon. Technol. Lett. **18**, 187 (2006).
19. Y. Liu, X. Feng, S. Yuan, et al., Opt. Express. **12**, 2056 (2004).
20. S. Pan and C. Lou, IEEE Photon. Technol. Lett. **18**, 604 (2006).
21. Y. D. Gong, M. Tang, P. Shum, et al., IEEE Photon. Technol. Lett. **17**, 2547 (2005).
22. S. Pan and C. Lou, IEEE Photon. Technol. Lett. **18**, 1451 (2006).
23. G. J. Cowle and D. Y. Stepanov, IEEE Photon. Technol. Lett. **8**, 1465 (1996).
24. J. W. Lou, T. F. Carruthers, and M. Currie, IEEE Photon. Technol. Lett. **16**, 51 (2004).
25. J. C. Travers, J. Morgenweg, E. D. Obraztsova, et al., Laser Phys. Lett. **8**, 144 (2011).
26. E. J. R. Kelleher, J. C. Travers, Z. Sun, et al., Laser Phys. Lett. **7**, 790 (2010).
27. M. R. A. Moghaddam, S. W. Harun, R. Akbari, and H. Ahmad, Laser Phys. Lett. **8**, 369 (2011).
28. M. J. Guy and J. R. Taylor, Electron. Lett. **29**, 2044 (1993).
29. D. U. Noske, M. J. Guy, K. Rottwitt, et al., Opt. Comm. **108**, 297 (1994).
30. H. Zhang, D. Y. Tang, X. Wu, and L. M. Zhao, Opt. Express. **17**, 12692 (2009).
31. X. Zhao, Z. Zheng, L. Liu, et al., Opt. Express. **19**, 1168 (2011).
32. D. Mao, X. M. Liu, L. R. Wang, et al., Laser Phys. **20**, 847 (2010).

33. A.-P. Luo, Z.-C. Luo, and W.-C. Xu, Laser Phys. **21**, 395 (2011).
34. A.-P. Luo, Z.-C. Luo, W.-C. Xu, et al., Laser Phys. Lett. **8**, 601 (2011).
35. W. C. Chen, Z. C. Luo, and W. C. Xu, Laser Phys. Lett. **6**, 816 (2009).
36. I. N. Duling III, Electron. Lett. **16**, 539 (1991).
37. N. J. Doran and D. Wood, Opt. Lett. **13**, 56 (1988).
38. E. A. Kuzin, N. Korneev, J. W. Haus, and B. Ibarra-Escamilla, J. Opt. Soc. Am., Ser. B **18**, 919 (2001).
39. O. Pottiez, E. A. Kuzin, B. Ibarra-Escamilla, and F. Mendez-Martinez, Opt. Comm. **254**, 152 (2005).
40. B. Ibarra-Escamilla, E. A. Kuzin, P. Zaca-Moran, et al., Opt. Express. **13**, 10760 (2005).
41. G. P. Agrawal, *Nonlinear Fiber Optics* (Academic, San Diego, 1995).
42. C. H. Yeh, C. W. Chow, Y. F. Wu, et al., Laser Phys. Lett. **8**, 672 (2011).
43. A. A. Latif, M. Z. Zulkifli, N. A. Awang, et al., Laser Phys. **20**, 2006 (2010).
44. A. W. Al-Alimi, M. H. Al-Mansoori, A. F. Abas, et al., Laser Phys. **20**, 2001 (2010).
45. M. Durán-Sánchez, A. Flores-Rosas, R. I. Álvarez-Tamayo, et al., Laser Phys. **20**, 1270 (2010).